Journal of Power Sources 240 (2013) 101–108

Contents lists available at SciVerse ScienceDirect

Journal of Power Sources

journal homepage: www.elsevier.com/locate/jpowsour

Spontaneous redox synthesis of Prussian blue/graphene nanocomposite as a non-precious metal catalyst for efficient four-electron oxygen reduction in acidic medium

Lei Xu, Guoquan Zhang*, Jie Chen, Yufei Zhou, Guang'en Yuan, Fenglin Yang*

Key Laboratory of Industrial Ecology and Environmental Engineering, Ministry of Education, School of Environmental Science and Technology, Dalian University of Technology, Linggong Road 2, Dalian 116023, PR China

HIGHLIGHTS

- Prussian blue/graphene (PB/GE) is synthesized by a spontaneous redox method.
- ORR occurs mainly inside the PB lattice via the $4e^-$ reduction pathway at $E > -0.5$ V.
- ORR occurs mainly on GE nanosheets via the "2 + 2" mechanism at $E < -0.5$ V.
- PB/GE exhibits favorable electrocatalytic activity and long-term stability toward ORR.

GRAPHICAL ABSTRACT

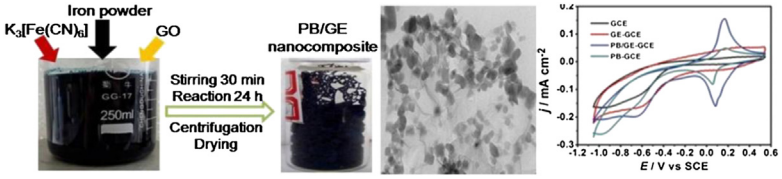

ARTICLE INFO

Article history:
Received 6 November 2012
Received in revised form
27 March 2013
Accepted 28 March 2013
Available online 9 April 2013

Keywords:
Electrocatalysis
Graphene
Oxygen reduction reaction
Prussian blue

ABSTRACT

A Prussian blue/graphene (PB/GE) nanocomposite is synthesized as a non-precious metal catalyst by a spontaneous redox reaction in acidic solution with Fe powder, $K_3[Fe(CN)_6]$, and graphene oxide as precursors. The resulting PB/GE nanocomposite is characterized by scanning electron microscopy, transmission electron microscopy, Raman spectroscopy, and X-ray photoelectron spectroscopy. The PB/GE nanocomposite-modified glassy carbon electrode (PB/GE–GCE) exhibits good electrocatalytic activity and long-term stability toward the oxygen reduction reaction (ORR). The reduced form of PB, Prussian white, has favorable electrocatalytic activity for the reduction of O_2 and H_2O_2 in acidic solutions. Rotating ring-disk voltammetric measurements clearly show that the dominant product of ORR at the PB–GCE is water produced by the $4e^-$ reduction of O_2 at all potentials. ORR at the PB/GE–GCE occurs mainly inside the PB lattice through the $4e^-$ reduction pathway at $E > -0.5$ V and on GE nanosheets through the "2 + 2" mechanism involving H_2O_2 as the intermediate product at $E < -0.5$ V. The PB/GE nanocomposite is a potentially efficient and cost-effective catalyst for fuel cells.

1. Introduction

Molecular oxygen is widely used as an electron acceptor for cathodes in many fuel cells because of its low cost, sustainability, and environment-friendliness [1–6]. Generally, the electrochemical oxygen reduction reaction (ORR) occurs via the $2e^-$, direct $4e^-$, or two $2e^-$ pathways ("2 + 2 mechanism"), depending on the electrode material, its surface properties, and the solution pH [7]. The $4e^-$ reduction process is ideal for fuel cells that acquire more electric energy. However, the kinetics of ORR is usually very slow, thereby limiting the practical applications of the reaction. Improving the design of electrocatalysts is thus very important to enhance the performance of cathodes, especially in fuel cells, by reducing the overpotential and achieving the $4e^-$ pathway of ORR.

* Corresponding authors. Tel./fax: +86 411 84706328.
E-mail addresses: guoquanz@126.com (G. Zhang), yangfl@dlut.edu.cn (F. Yang).

0378-7753/$ – see front matter © 2013 Elsevier B.V. All rights reserved.
http://dx.doi.org/10.1016/j.jpowsour.2013.03.156

Prussian blue (PB) has a face-centered cubic structure in which alternating Fe^{II} and Fe^{III} centers are bridged by cyanide ions in a Fe^{II}–C≡N–Fe^{III} fashion, forming an infinite three dimensional network [8]. Itaya et al. [9] first found that PB-modified electrodes have excellent electrocatalytic activity for ORR in acidic aqueous solutions. The ORR mechanism of the PB-modified electrode includes two fundamental steps. First, PB is reduced at the cathode, and the reduced form of the polycrystal is denoted as Prussian white (PW) [10]. Second, PW is oxidized into PB by O_2 with the simultaneous formation of water [9]. These steps are described in Eqs. (1) and (2) as follows:

$$Fe_4^{3+}\left[Fe^{II}(CN)_6\right]_3 + 4e^- + 4K^+ \rightarrow K_4^+Fe_4^{2+}\left[Fe^{II}(CN)_6\right]_3 \quad (1)$$

$$K_4Fe_4^{2+}\left[Fe^{II}(CN)_6\right]_3 + O_2 + 4H^+ \rightarrow Fe_4^{3+}\left[Fe^{II}(CN)_6\right]_3 + 2H_2O + 4K^+ \quad (2)$$

where Fe^{3+} and Fe^{II} are the high-spin and low-spin Fe ions, respectively.

Graphene (GE), a new class of two-dimensional nanomaterials consisting of a single layer of C atoms with an sp^2 network, has recently received increased research attention because of its unique nanostructure, excellent electron-transfer capacity, high stability, and large accessible surface area [6,11]. GE nanosheets can be facilely obtained from graphene oxide (GO) by different reduction methods, such as hydrothermal reduction [11–14], chemical vapor deposition [15], chemical reduction [16–19], electrochemical reduction [6,20], and microbial reduction [21].

Fan et al. [18] synthesized GE nanosheets based on Fe reduction of exfoliated GO via a green and facile approach. The present study also synthesizes a PB/GE nanocomposite in situ by a spontaneous redox reaction in an acidic aqueous solution containing Fe powder, $K_3[Fe(CN)_6]$, and GO as precursors. The resulting nanocomposite was characterized by scanning electron microscopy (SEM), transmission electron microscopy (TEM), Raman spectroscopy, and X-ray photoelectron spectroscopy (XPS). The electrocatalytic ORR on the PB/GE nanocomposite was evaluated by cyclic voltammetry (CV), chronocoulometry/chronoamperometry, and the rotating ring-disk electrode (RRDE) method in acidic medium.

2. Experimental

2.1. Reagents

Graphite powder (325 mesh, spectrum pure), $K_3[Fe(CN)_6]$, $NaNO_3$, KCl, K_2SO_4, and Fe powder (average particle size: 10 μm) were obtained from Shanghai Chemical Reagent Co. (China). H_2O_2 (30 wt%) and other reagents were purchased from Beijing Chemical Reagent Plant (China). All of the reagents employed in the experiment were of analytical grade and used as received without further purification. Aqueous solutions were prepared with double-distilled water from a Millipore system (>18 MΩ cm).

2.2. Synthesis of PB/GE nanocomposite

GO was synthesized from natural graphite powder using a modified Hummers method [22,23]. The PB/GE nanocomposite was prepared by a spontaneous one-pot redox synthesis method. The general synthesis procedure for the PB/GE nanocomposite is described in Scheme 1. Briefly, 1.0 g of Fe powder, 1.0 g of $K_3[Fe(CN)_6]$, and 30 mL of HCl (35 wt%) were directly added to 100 mL of a GO suspension (0.5 mg mL^{-1}) at ambient temperature. The mixture was stirred for 30 min to ensure complete homogeneity and then allowed to stand for 24 h. The brown GO rapidly darkened in color in the presence of both Fe powder and H^+. After reduction, 20 mL of HCl (35 wt%) was again added to the solution to completely remove the excess Fe powder. Finally, the mixture was centrifuged, washed several times with pure water and ethanol, and then dried at 60 °C for 12 h in a vacuum oven. For comparison, GE and PB nanocomposites were also synthesized by the same method, except that the $K_3[Fe(CN)_6]$ and GO suspensions were changed to double-distilled water.

2.3. Characterization

SEM images were obtained using an XL30 ESEM FEG SEM instrument operating at 5 kV. TEM images were obtained using a JEOL JEM-2000 EX TEM instrument by dropping the complex solution onto Cu grids. Raman spectra were collected using a Renishaw inVia M2000 spectrometer (UK) operating with He–Ne laser excitation at a wavelength of 623.8 nm, laser power of 35 mW, and beam spot size of about 2 μm. XPS analysis was performed on an ESCALAB MK II X-ray photoelectron spectrometer.

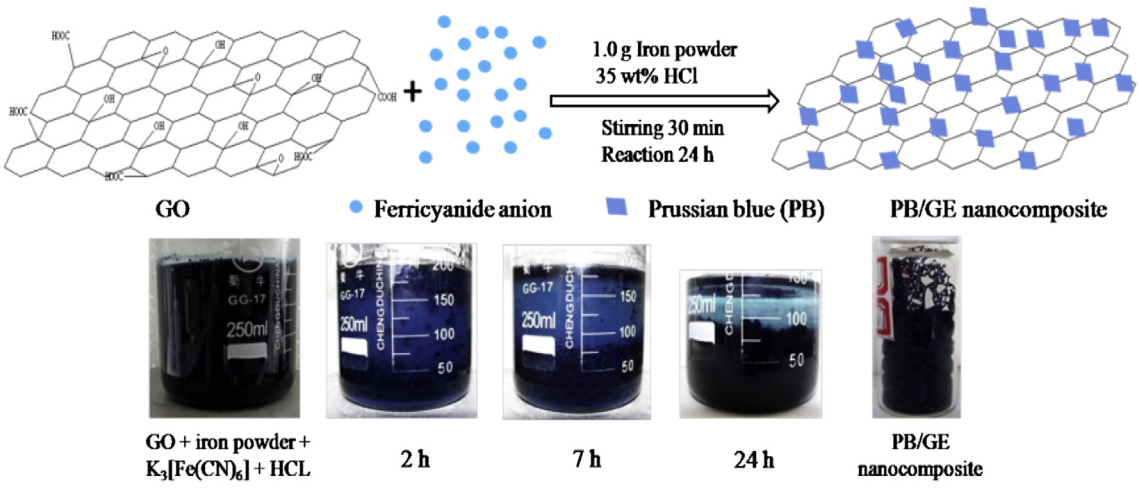

Scheme 1. Synthesis procedure of the PB/GE nanocomposite.

2.4. Preparation of modified electrodes

Prior to surface modification, a glassy carbon electrode (GCE, Φ = 5 mm) was polished to a mirror-like surface with alumina particles down to 0.05 μm, rinsed with Millipore water, and sonicated successively in 1:1 HNO_3, acetone, and pure water. The pretreated GCE was allowed to dry under N_2. The PB/GE nanocomposite-modified GCE electrode was prepared as follows. Briefly, PB/GE nanocomposite powders were first dispersed in ethanol to yield 2 mg mL^{-1} homogeneous suspensions. Subsequently, 2 μL of the suspensions was cast onto the GCE surface and allowed to dry in air. This process was repeated five times for CV and electrochemical impedance spectroscopy (EIS) and ten times for the RRDE experiment. The as-prepared electrodes were denoted as PB/GE–GCE. Similarly, PB film and GE nanosheet-modified GCE electrodes were also synthesized and denoted as PB–GCE and GE–GCE, respectively.

2.5. Electrocatalytic activities

Electrochemical measurements were conducted in a conventional three-electrode system, with a Pt sheet (surface area 4 cm^2) as the counter electrode and a saturated calomel electrode as the reference electrode. CV, EIS, and RRDE measurements were used to study the electrochemical behaviors and electrocatalytic activities of the bare GCE, GE–GCE, PB–GCE, and PB/GE–GCE. CV and chronocoulometry/chronoamperometry measurements were conducted using an EG&G PARC Model 263A potentiostat–galvanostat (Princeton, NJ, USA) controlled by a general-purpose electrochemical system software. The EIS experiment was performed using an EG&G PARC frequency response detector (FRD 100) and recorded at frequencies ranging from 100 kHz to 10 mHz with an AC signal potential amplitude of 10 mV and applied potential of 0 V. Nyquist representations of the impedance data were analyzed using ZSimpWin V3.10 software. RRDE was performed using a CHI 730D electrochemical analyzer combined with an EG&G PARC Model 636 electrode rotator system.

3. Results and discussion

3.1. Characterization of the PB/GE nanocomposite

Fig. 1A and B show the morphology of the PB/GE nanocomposite as investigated by SEM and TEM, respectively. The SEM image of the PB/GE nanocomposite revealed that large quantities of cubic PB nanoparticles on the GE nanosheets were highly uniform. The TEM image showed that most of the PB nanoparticles had an average size of approximately 50 nm and were randomly deposited on the silk-like surface of the GE nanosheets, indicating the successful generation of the PB/GE nanocomposite by a facile one-pot spontaneous redox synthesis method.

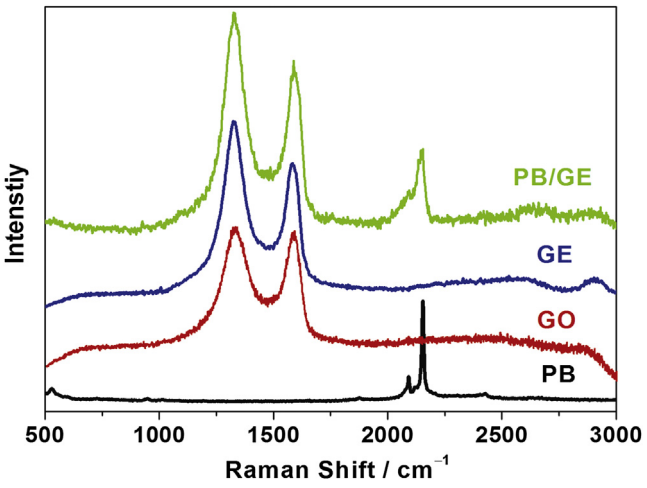

Fig. 2. Raman spectra of the PB, GO, GE, and PB/GE nanocomposites.

Fig. 2 shows the Raman spectra of PB, GO, GE, and PB/GE nanocomposites. The strong vibrational band at 2095 cm^{-1} was assigned to the stretching vibration of the C–N group of PB [24], indicating the presence of PB on the GE surface. Compared with GO, the D and G bands of GE showed red-shifts (in web version) from 1322 to 1582 cm^{-1} to 1327 and 1593 cm^{-1}, respectively. The D/G ratio was increased with the prominence of the D band, which is consistent with the Raman spectra of GO chemically reduced by hydrazine in a previous study [16]. The D and G bands of the PB/GE nanocomposite were similar to those of GE nanosheets but an additional band was observed at 2095 cm^{-1}, demonstrating the transformation of GO to GE during the spontaneous redox process.

Fig. 3A and B show the fully scanned XPS spectra of GO and PB/GE nanocomposites, respectively. Only C and O elements were observed in GO, and the O element existed mainly in the forms of hydroxyl, epoxide, carboxylic, and carbonyl groups [18,21]. After spontaneous redox reaction in the presence of Fe powders, $K_3Fe(CN)_6$, and GO, N and Fe elements were observed in the XPS spectrum of the PB/GE nanocomposite in addition to C and O elements, thereby confirming the presence of C–N ($[Fe(CN)_6]^{4-}$) in the as-synthesized PB/GE nanocomposite.

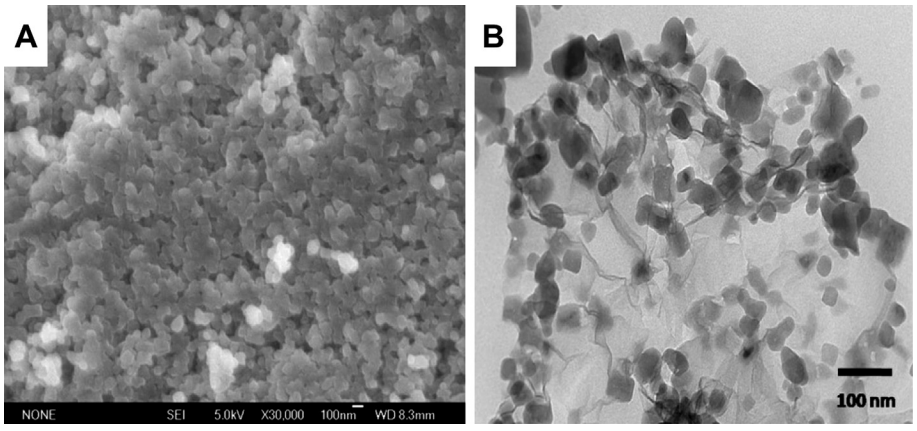

Fig. 1. (A) SEM and (B) TEM images of the PB/GE nanocomposite.

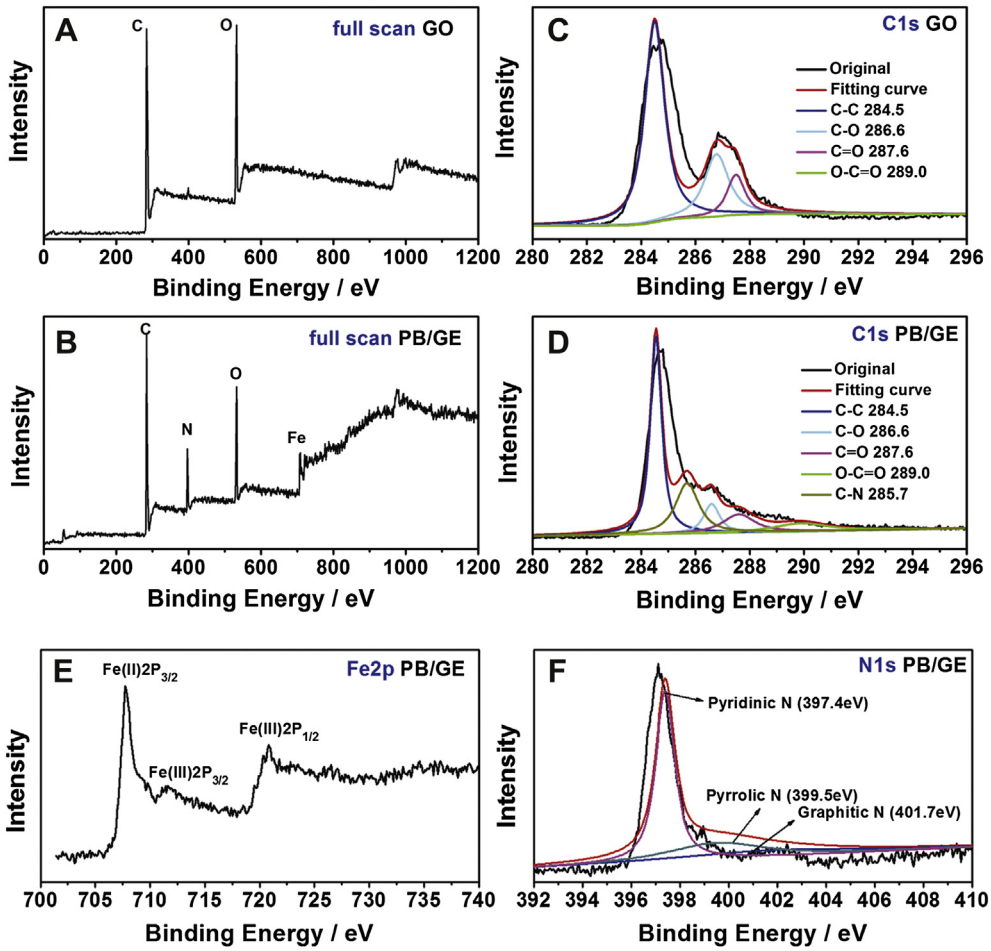

Fig. 3. Full scan XPS spectra of (A) GO and (B) PB/GE nanocomposites. C1 XPS spectra of (C) GO and (D) PB/GE nanocomposites. (E) Fe2p and (F) N1 XPS spectra of the PB/GE nanocomposite.

To further understand the electronic states of the elements, the high-resolution C1 peaks of GO and PB/GE were investigated. Fig. 3C and D shows that four types of C with different chemical states may be observed at 284.5 (C–C), 286.6 (C–O), 287.6 (C=O), and 289.0 eV (O–C=O). The PB/GE spectrum shows that the oxygenated C peaks became significantly weaker with the increase in the sp^2 C peak, proving that the hydroxyl, epoxide, carboxylic, and carbonyl groups were effectively eliminated in the reduction process. The peak at 285.8 eV is attributed to the C–N bond of PB/GE. The binding energies of $Fe2p_{3/2}$ and $Fe2p_{1/2}$ appeared at 711.3 and 721.8 eV, respectively, and originated from the presence of Fe^{3+} [25]. Fig. 3E shows the peak at 708.3 eV assigned to $Fe2p_{3/2}$ of Fe(II) [26]. Fig. 3F shows high-resolution N1 peaks in the XPS spectra fitted with three components originating from graphitic (401.7 eV), pyrrolic (399.5 eV), and pyridinic (397.4 eV) N, indicating the presence of C–N ($[Fe(CN)_6]^{3-}$) in the hybrids. The higher resolution spectra of Fe2p and N1s indicate that the PB nanoparticles were synthesized successfully.

3.2. Electrochemical properties in the $K_3[Fe(CN)_6]$ solution

The $[Fe(CN)_6]^{3-/4-}$ redox couple is an excellent redox probe used to investigate the heterogeneous electron transfer rate and nature of the interaction between different molecules and electrode surfaces. Fig. 4A shows the electrochemical properties of the bare GCE, GE–GCE, PB–GCE, and PB/GE–GCE in 0.1 mol L^{-1} KCl solution containing 2 mmol L^{-1} $K_3[Fe(CN)_6]$. The redox peak current of the $[Fe(CN)_6]^{3-/4-}$ probe on the GE–GCE was larger than those on the GCE and PB–GCE. The formal potentials ($E^{0'} = (E_{pa} + E_{pc})/2$) of all four electrodes were almost constant. The increased electroactivity of the PB/GE–GCE toward the $[Fe(CN)_6]^{3-/4-}$ probe is attributed to the superior electronic property of the GE nanosheets and the mediated electron transfer with redox centers in PB.

The electroactive surface area of the PB/GE–GCE may be estimated according to the Randles-Sevcik equation as follows [27]:

$$I_p = 2.69 \times 10^5 AcD^{1/2}n^{3/2}v^{1/2} \quad (3)$$

where I_p is the peak current of different scan rates, c is the concentration of $K_3[Fe(CN)_6]$ (mol L^{-1}), D is the diffusion coefficient of $K_3[Fe(CN)_6]$ (cm^2 s^{-1}), n is the number of transferred electrons for the $[Fe(CN)_6]^{3-/4-}$ redox couple ($n = 1$), and v is the scan rate (V s^{-1}). The electroactive surface area was calculated as ca. 0.434 cm^2 based on the slope of I_p vs. $v^{1/2}$ of Fig. 4B.

Fig. 4C and D shows the favorable electrochemical properties of the PB/GE nanocomposite as verified using EIS. The charge transfer resistances (R_{ct}) of the $[Fe(CN)_6]^{3-/4-}$ redox probe measured as the diameter of the semicircle in the Nyquist plots were ca. 98.43, 471.8, 158.3, and 104.6 Ω for the bare GCE, PB–GCE, GE–GCE, and PB/GE–GCE, respectively. The R_{ct} of the PB/GE–GCE was much smaller than that of the PB–GCE, implying fast electron transfer kinetics in the

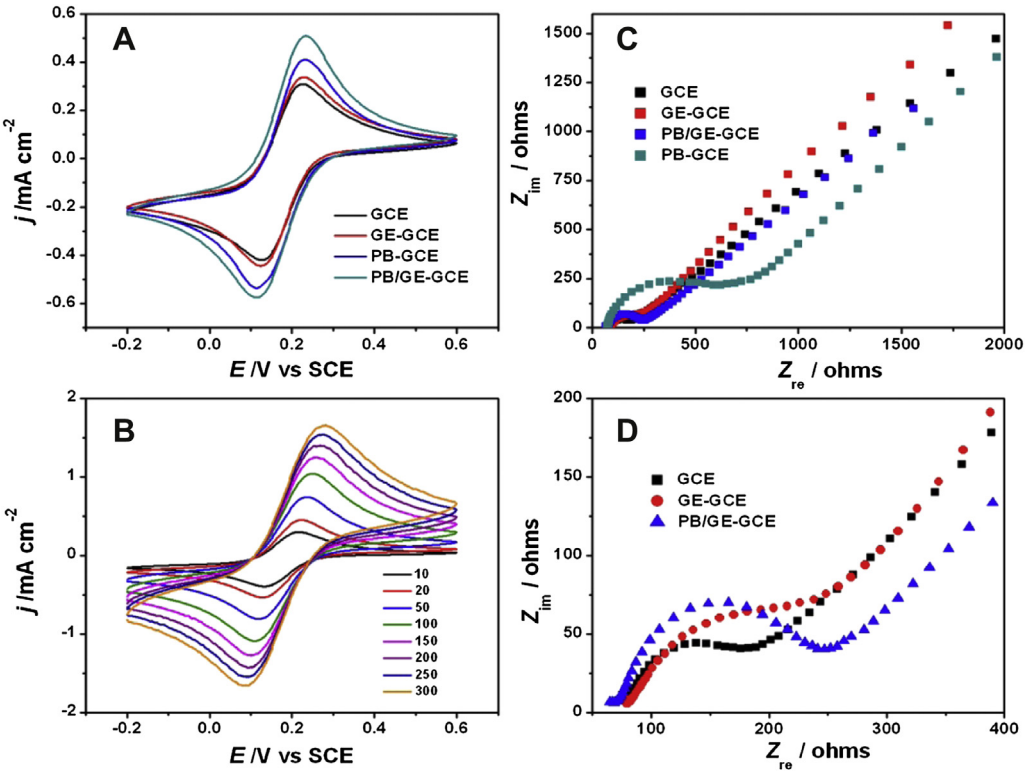

Fig. 4. (A) CV and (C) Nyquist diagrams of the bare GCE, GE–GCE, PB–GCE, and PB/GE–GCE in 2.0 mmol L^{-1} $K_3[Fe(CN)_6]$ solution containing 0.1 mol L^{-1} KCl as the supporting electrolyte. (B) CV of the PB/GE–GCE at different scan rates. (D) Local amplification of Nyquist diagrams of the GCE, GE–GCE, and PB/GE–GCE. Scan rate: 20 mV s^{-1}.

presence of GE nanosheets. These results suggest that the PB/GE nanocomposite presents potential benefits toward ORR because of its excellent electrocatalytic performance.

3.3. CV study of the ORR

Fig. 5A shows the CV results of the bare GCE, GE–GCE, PB–GCE, and PB/GE–GCE in N_2-saturated 0.1 mol L^{-1} H_2SO_4 solution containing 0.1 mol L^{-1} K_2SO_4. The redox peaks at ca. 0.13 V characterized by the quasi-reversible electron transfer process were caused by redox transformation between PB and its reduced form, PW, as shown in the Eq. (1). In addition, in situ Müssbauer measurements show that the reduction of PB at ca. 0.17 V was caused by the electron-transfer reaction of the high-spin Fe ions (Fe^{3+}) in PB [28]. Similar to the results obtained in the $K_3[Fe(CN)_6]$ solution, the PB/GE–GCE exhibited larger redox peak currents than the PB–GCE. This result can be attributed to the larger surface area and higher electron communication capability of the GE nanosheets, which play a key role in facilitating the direct electron transfer of the PB/PW redox couple, such as in promoting the reduction of Fe^{3+} to Fe^{2+} [29–32].

Fig. 5B shows the CV results of the bare GCE, GE–GCE, PB–GCE, and PB/GE–GCE in O_2-saturated 0.1 mol L^{-1} H_2SO_4 solution containing 0.1 mol L^{-1} K_2SO_4. O_2 reduction began at ca. −0.25 V for the bare GCE, and an ill-defined O_2 reduction peak was observed in the potential range of −0.7 V to −0.5 V. These findings agree well with previous studies [33–35] showing that carbon materials can efficiently catalyze O_2 reduction in this potential range through mediation by active quinone-like groups on the GCE surface. Compared with the bare GCE, reduction of O_2 began at ca. −0.2 V for the GE–GCE, and a notable increase in O_2 reduction current was observed at potentials ranging from −0.7 V to −0.5 V. These results indicate the improved electrocatalytic activity of the GE–GCE toward ORR compared with the bare GCE.

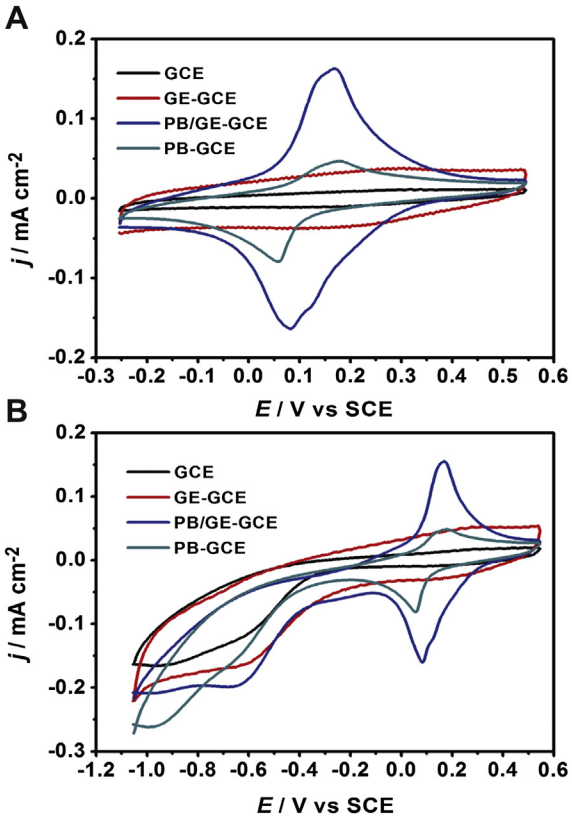

Fig. 5. CVs of the bare GCE, GE–GCE, PB–GCE, and PB/GE–GCE in (A) N_2-saturated and (B) O_2-saturated 0.1 mol L^{-1} H_2SO_4 containing 0.1 mol L^{-1} K_2SO_4 as the electrolyte. Scan rate: 20 mV s^{-1}.

The O_2 reduction onset potential for the PB–GCE was similar to that of the bare GCE; a more pronounced reduction current was also obtained in the potential range of −0.7 V to −0.5 V for the PB–GE. This increased current may be ascribed to O_2 reduction in the interface between the PB film and GCE as described by Itaya et al. [9], where unreacted O_2 molecules diffuse through the PB crystals and are then reduced at the GCE surface. Compared with the PB film and GE nanocomposite-modified GCEs, the catalytic reduction current of O_2 for the PB/GE–GCE began at approximately −0.2 V, similar to that for the GE–GCE. The PB/GE–GCE has the functions of both GE nanosheets and PB films, resulting in a higher background currents, stronger PB/PW redox peaks, and better electrocatalytic activities toward O_2 reduction. Similarly, a larger catalytic reduction current was also observed at potentials ranging from −0.7 V to −0.5 V for the PB/GE–GCE. This increased current is caused by spontaneous O_2 reduction that occurs to form H_2O_2 on the GE nanosheets of PB/GE nanocomposite, in addition to unreacted O_2 molecules passing through the PB crystal and then becoming reduced at the GE–GCE surface. The correspondence between the O_2 reduction potential and the formal potential of the PB/PW redox couple indicates that the high-spin Fe ions in PB, Fe^{3+}, have catalytic activity toward ORR. Thus, Fe^{3+}/Fe^{2+}, as a redox mediator system, is involved in the reduction of O_2.

3.4. Chronocoulometry study of ORR

Quantitative assessment of the number of transferred electron, n, involved in ORR was performed by chronocoulometry according to Eq. (4) as follows:

$$Q = 2nFAc_{O_2}D^{1/2}\pi^{-1/2}t^{1/2} \quad (4)$$

where Q is the experiment value of charge, A is the surface area of GCE (cm^2), c_{O_2} is the concentration of dissolved O_2 (mol L^{-1}), and D is the diffusion coefficient of dissolved O_2 (cm^2 s^{-1}).Fig. 6A shows the plot of Q vs. $t^{1/2}$ for the PB/GE–GCE in the O_2-saturated electrolyte. The inset of Fig. 6A shows the corresponding chronocoulometric curve, in which the electrode potential was stepped from 0.2 V to −0.4 V. The number of transferred electrons involved in ORR, n, calculated from the slopes of the chronocoulometric plots was 3.74 for the PB/GE–GCE. Fig. 6B shows that the value of n was 2.32 for the GE–GCE when the cathodic potential was stepped from 0 V to −0.6 V. This result proves that O_2 reduction on the PB/GE–GCE proceeds through a $4e^-$ reduction pathway, while that on the GE–GCE proceeds through a $2e^-$ reduction pathway that produces H_2O_2 in the potential step range studied. The PB/GE nanocomposite is thus a potential non-precious metal catalyst that may be used as a promising cathode modifier for fuel cells.

3.5. RRDE study of ORR

RRDE is often used to study the possible pathways of ORR [36,37]. Fig. 7 shows the electrocatalytic activities of the bare GCE, GE–GCE, PB–GCE, and PB/GE–GCE toward ORR at a rotation speed of 1000 rpm and scan rate of 10 mV s^{-1}. The Pt ring electrode was held at a potential of +1.0 V to detect any H_2O_2 formed at the disk electrode. The anodic currents for the bare GCE and GE–GCE were simultaneously observed at the Pt ring electrode, showing H_2O_2 as the dominant product of ORR in the potential range studied. This result agrees well with findings in previous studies [38,39]. The disk and ring currents of the GE–GCE were larger than those of the bare GCE at potentials ranging from ca. −0.85 V to −0.25 V, which can be attributed to the larger surface area and higher electrochemical activity of the rough GE–GCE. However, the ring current of the GE–GCE was lower than that of the GCE at potentials lower than −0.85 V, indicating the reduction of H_2O_2 to water on the GE–GCE surface.

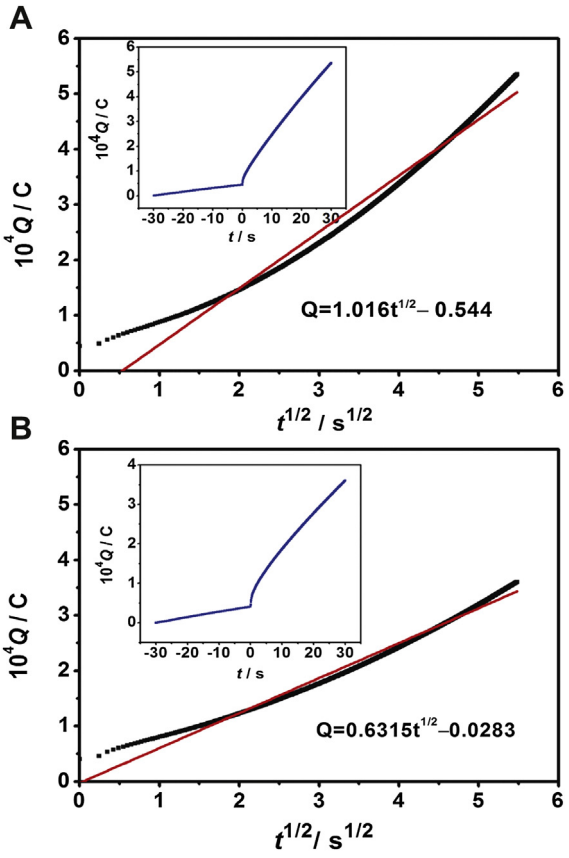

Fig. 6. Plot of Q vs. $t^{1/2}$ for the (A) PB/GE–GCE and (B) GE–GCE in O_2-saturated 0.1 mol L^{-1} H_2SO_4 containing 0.1 mol L^{-1} K_2SO_4 as the electrolyte. The insets show the corresponding chronocoulometric curves.

No detectable anodic ring current was measured for the PB–GCE in the potential range investigated, indicating that the dominant

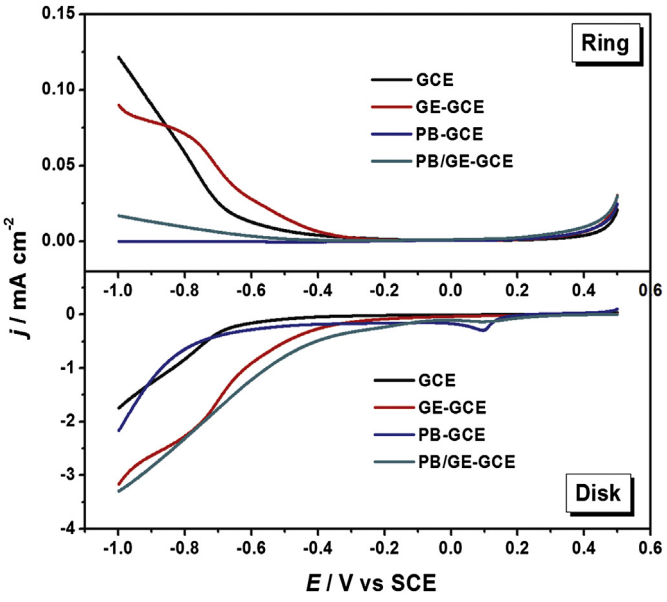

Fig. 7. RRDE data of the bare GCE, GE–GCE, PB–GCE, and PB/GE–GCE in O_2-saturated 0.1 mol L^{-1} H_2SO_4 containing 0.1 mol L^{-1} K_2SO_4 as the electrolyte at a rotating rate of 1000 rpm. Scan rate: 10 mV s^{-1}.

product of ORR in PB–GCE is water, similar to the report by Itaya et al. [9]. A possible mechanism for these results is production of the dominant product of ORR, water, by the direct $4e^-$ reduction of O_2 at the PB–GCE, as shown in Eq. (2). Another possible mechanism is the "2 + 2" mechanism, as shown in Eqs. (5) and (6).

$$K_4Fe_4^{2+}\left[Fe^{II}(CN)_6\right]_3 + O_2 + 2H^+ \rightarrow K_2Fe_2^{3+}Fe_2^{2+}\left[Fe^{II}(CN)_6\right]_3 \cdot H_2O_2 + 2K^+ \quad (5)$$

$$K_2Fe_2^{3+}Fe_2^{2+}\left[Fe^{II}(CN)_6\right]_3 \cdot H_2O_2 + 2H^+ \rightarrow Fe_4^{3+}\left[Fe^{II}(CN)_6\right]_3 \cdot H_2O_2 + 2H_2O + 2K^+ \quad (6)$$

In the second pathway, H_2O_2 is considered an intermediate species. The nonappearance of H_2O_2 oxidation currents in the RRDE may be explained by the assumption that all of the formed H_2O_2 is completely reduced to water in the PB lattice before it diffuses out of the PB crystal.

The PB/GE–GCE showed a weak ring current at the potential that was more negative than −0.5 V, suggesting that the reduction product contains some amount of H_2O_2. This result can be explained by the spontaneous reduction of dissolved O_2 molecules to generate the dominant product, H_2O_2, on the GE nanosheets of the PB/GE nanocomposite. The reduction of H_2O_2 produces water on the GE–GCE surface at potentials more negative than −0.85 V. The H_2O_2 formed in the PB lattice can be completely reduced to water before it diffuses out of the PB crystals, resulting in the ring current being merely 1% of the disk current. Compared with the PB–GCE, the increase in disk current of the PB/GE–GCE is attributed to the presence of GE nanosheets, which provide large surface areas, rapid electron transfers, low internal resistances, and higher electrocatalytic activities.

The electrocatalytic activities of other GE-based electrodes using different modification strategies toward O_2 reduction are summarized in Table 1. The table illustrates that the electrocatalytic activity of the PB/GE nanocomposite synthesized by the proposed strategy is comparable with or better than that of other GE-based nanomaterial-modified electrodes.

To determine the long-term stability of the PB/GE, chronoamperometry tests were conducted in O_2-saturated 0.1 mol L^{-1} H_2SO_4 containing 0.1 mol L^{-1} K_2SO_4 as the electrolyte at room temperature and constant potentials of 0.15 and −0.3 V for 5400 s. Fig. 8 shows that the PB/GE nanocomposite synthesized by the proposed spontaneous redox reaction exhibited good reproducibility after long-term operation at +0.15 V, whereas the O_2 reduction current at −0.3 V decreased slightly. The low operational stability can be explained by inactivation during the electrocatalytic reaction. The product of the electrochemical reduction of O_2 at this potential can gradually transfer to hydroxide ions, which are able to solubilize a small amount of PB, with increasing time [40].

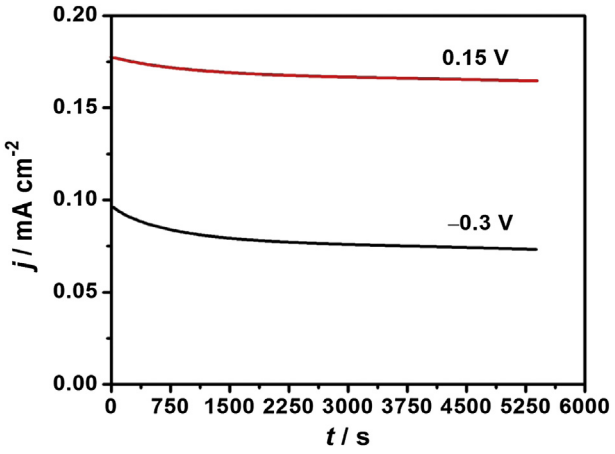

Fig. 8. Chronoamperograms of PB/GE–GCE in O_2-saturated 0.1 mol L^{-1} H_2SO_4 containing 0.1 mol L^{-1} K_2SO_4 as the electrolyte at operation potentials of +0.15 and −0.3 V at room temperature for 5400 s.

3.6. CV study of the ORR pathway

To further explain the ORR mechanism on the PB/GE–GCE, CV was again performed in N_2- and O_2-saturated 0.1 mol L^{-1} H_2SO_4 solution with or without 0.5 mmol L^{-1} H_2O_2. Fig. 9 shows that the catalyzed reduction current of H_2O_2 in the N_2-saturated electrolyte began at approximately 0.1 V (*curve c*), where the high-spin Fe ions in PB, Fe^{3+}, was reduced to Fe^{2+} (*curve a*). PB can be used as an ideal sensor for detecting H_2O_2 at potentials ranging from −0.1 V to 0.15 V [40–42], which suggests that H_2O_2 molecules are able to diffuse into the PB crystals and become reduced by Fe^{2+} centered in PB.

In the O_2-saturated solution, the catalytic reduction current in *curve c* was larger than that in *curve b* at potentials more positive than −0.5 V, which confirms that the catalytic reduction of H_2O_2 to water occurs faster than the catalytic reduction of O_2 to H_2O_2 at the PB/GE–GCE in this potential range. In addition, the reduction current of *curve d* was larger than that of *curves b* and *c* and almost equal to their stacking values, indicating that both O_2 and H_2O_2 molecules can simultaneously diffuse through PB crystals and become reduced on the PB/GE–GCE.

The mechanism of the catalyzed O_2 reaction on the PB/GE–GCE combined with the results of RRDE is described below.

First, ORR occurs mainly inside the PB lattice at cathodic potentials more positive than −0.5 V through two possible mechanisms. On the one hand, O_2 molecules receive $4e^-$, leading to formation of water, as shown in Eq. (2). On the other hand,

Table 1
Comparison in the electrocatalytic performance of various graphene-based nano-materials toward the ORR with PB/GE.

Catalytic electrode material	Synthesis method	Electrolyte	ORR onset potential	ORR pathway	Ref.
Fe–N–rGO	Heat treatment	PBS	0.22 V vs. SCE	4-Electron	[1]
Fe–N–rGO	Hydrothermal	0.5 M H_2SO_4	0.75 V vs. NHE	4-Electron	[14]
Fe_3O_4/N–GAs	Hydrothermal	0.1 M KOH	−0.19 V	4-Electron	[13]
Fe_3O_4/N–GSs			−0.26 V vs. Ag/AgCl		
N–graphene	CVD	0.1 M KOH	−0.2 V vs. Ag/AgCl	4-Electron	[15]
N–graphene	Heat treatment	0.1 M KOH	0.046 V vs. NHE	4-Electron	[3]
(G-dye-FeP)$_n$ MOF	Hydrothermal	0.1 M KOH	−0.15 V vs. Ag/AgCl	4-Electron	[11]
AQ/rGO	Electro-reductive	PBS (pH = 7.0)	−0.3 V vs. SCE	2-Electron	[6]
PB/GE	Spontaneous redox synthesis	0.1 M H_2SO_4	−0.2 V vs. SCE	4-Electron	Present work

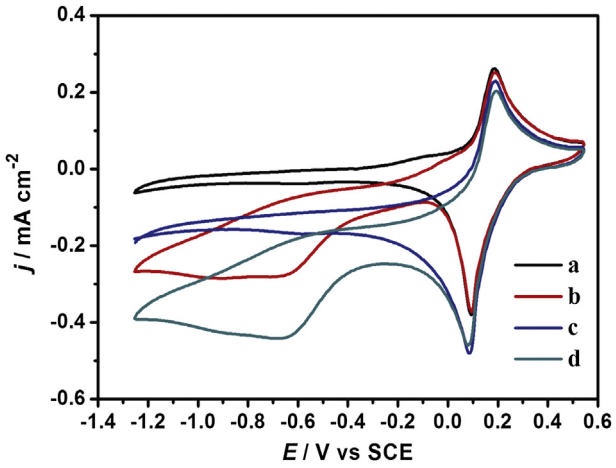

Fig. 9. CVs of PB/GE–GCE in 0.1 mol L^{-1} H_2SO_4 containing 0.1 mol L^{-1} K_2SO_4 as the electrolyte under various conditions as follows: (a) N_2-saturated, (b) O_2-saturated, (c) N_2-saturated + 0.5 mmol L^{-1} H_2O_2, and (d) O_2-saturated + 0.5 mmol L^{-1} H_2O_2. Scan rate: 20 mV s^{-1}.

reduction of O_2 may also occur at the interface between the PB and GE–GCE, where unreacted O_2 molecules pass through the PB lattice and are reduced to H_2O_2 on the GE–GCE surface. The H_2O_2 formed is then rapidly and completely reduced to water in the PB lattice before diffusing out of the PB crystals, as shown in Eqs. (5) and (6).

Second, ORR occurs mainly on the GE–GCE surface at cathodic potentials more negative than −0.5 V through the following mechanisms:

$$O_2 + 2H^+ + 2e^+ \rightarrow H_2O_2 \quad (7)$$

$$H_2O_2 + 2H^+ + 2e^+ \rightarrow 2H_2O \quad (8)$$

The dissolved O_2 molecules may be reduced spontaneously to H_2O_2 on the GE nanosheets of PB/GE nanocomposite at $E < -0.5$ V. Most of the formed H_2O_2 could be further reduced to water by GE nanosheets at more negative cathodic potentials.

4. Conclusion

In summary, a PB/GE nanocomposite was synthesized in situ by a spontaneous redox reaction in acidic solution containing Fe powder, $K_3[Fe(CN)_6]$, and GO as precursors. SEM, TEM, Raman, and XPS spectra results confirmed that GO is reduced to GE and that the Fe powder is oxidized to Fe^{2+}, which could react with $Fe(CN)_6^{3-}$ to produce PB. Electrochemical experiments indicated that the PB/GE nanocomposite has favorable electrochemical activity and stability. Introduction of GE increased the electroactive surface area and facilitated electron transfer because of the high electric conductivity of GE. RRDE experiments proved that ORR on the PB/GE nanocomposite-modified GCE electrode proceeds through the $4e^-$ reduction pathway at $E > -0.5$ V, followed by the "2 + 2" mechanism with H_2O_2 as the intermediate product at $E < -0.5$ V. These results suggest that the proposed one-pot spontaneous redox synthesis method is a facile strategy for preparing PB/GE nanocomposites that may be used as promising candidates for efficient and cost-effective catalysts in fuel cells.

Acknowledgments

The authors would like to acknowledge the National Natural Science Foundation of China (No. 21177017 and 21177019) and the Post-Doctoral Science Foundation of China (No. 2011M500560) for their financial support.

References

[1] Y. Hu, Q. Xu, J. Sun, B. Hou, Y. Zhang, J. Power Sources 213 (2012) 265–269.
[2] J. Mao, L. Yang, P. Yu, X. Wei, L. Mao, Electrochem. Commun. 19 (2012) 29–31.
[3] D.S. Geng, Y. Chen, Y.G. Chen, Y.L. Li, R.Y. Li, X.L. Sun, S.Y. Ye, S. Knights, Energy Environ. Sci. 4 (2011) 760–764.
[4] J. Wu, D. Zhang, Y. Wang, Y. Wan, B. Hou, J. Power Sources 198 (2012) 122–126.
[5] W. Zhang, A.U. Shaikh, E.Y. Tsui, T.M. Swager, Chem. Mater. 21 (2009) 3234–3241.
[6] Y.F. Zhou, G.Q. Zhang, J. Chen, G. Yuan, L. Xu, L.F. Liu, F.L. Yang, Electrochem. Commun. 22 (2012) 69–72.
[7] B. Šljukić, C. Banks, R. Compton, J. Iran. Chem. Soc. 2 (2005) 1–25.
[8] J. Keggin, F. Miles, Nature 137 (1936) 577–578.
[9] K. Itaya, N. Shoji, I. Uchida, J. Am. Chem. Soc. 106 (1984) 3423–3429.
[10] A.A. Karyakin, Electroanalysis 13 (2001) 813–819.
[11] M. Jahan, Q. Bao, K.P. Loh, J. Am. Chem. Soc. 134 (2012) 6707–6713.
[12] M.J. McAllister, J.L. Li, D.H. Adamson, H.C. Schniepp, A.A. Abdala, J. Liu, M. Herrera-Alonso, D.L. Milius, R. Car, R.K. Prudhomme, Chem. Mater. 19 (2007) 4396–4404.
[13] Z.-S. Wu, S.B. Yang, Y. Sun, K. Parvez, X.L. Feng, K. Müllen, J. Am. Chem. Soc. 134 (2012) 9082–9085.
[14] H.R. Byon, J. Suntivich, S.-H. Yang, Chem. Mater. 23 (2011) 3421–3428.
[15] L.T. Qu, Y. Liu, J.-B. Baek, L.M. Dai, ACS Nano 4 (2010) 1321–1326.
[16] S. Stankovich, D.A. Dikin, R.D. Piner, K.A. Kohlhaas, A. Kleinhammes, Y. Jia, Y. Wu, S.B.T. Nguyen, R.S. Ruoff, Carbon 45 (2007) 1558–1565.
[17] H.J. Shin, K.K. Kim, A. Benayad, S.M. Yoon, H.K. Park, I.S. Jung, M.H. Jin, H.K. Jeong, J.M. Kim, J.Y. Choi, Adv. Funct. Mater. 19 (2009) 1987–1992.
[18] Z.J. Fan, W. Kai, J. Yan, T. Wei, L.J. Zhi, J. Feng, Y. Ren, L.P. Song, F. Wei, ACS Nano 5 (2011) 191–198.
[19] Y. Wang, Z. Shi, J. Yin, ACS Appl. Mater. Interfaces 3 (2011) 1127–1133.
[20] M. Zhou, Y. Wang, Y. Zhai, J. Zhai, W. Ren, F. Wang, S. Dong, Chem. Eur. J. 15 (2009) 6116–6120.
[21] G. Wang, F. Qian, C.W. Saltikov, Y. Jiao, Y. Li, Nano Res. 4 (2011) 563–570.
[22] W.S. Hummers Jr., R.E. Offeman, J. Am. Chem. Soc. 80 (1958), 1339–1339.
[23] N.I. Kovtyukhova, P.J. Ollivier, B.R. Martin, T.E. Mallouk, S.A. Chizhik, E.V. Buzaneva, A.D. Gorchinskiy, Chem. Mater. 11 (1999) 771–778.
[24] L. Xia, R.L. McCreery, J. Electrochem. Soc. 146 (1999) 3696–3701.
[25] T. Uemura, M. Ohba, S. Kitagawa, Inorg. Chem. 43 (2004) 7339–7345.
[26] P. Diao, Z. Liu, B. Wu, X. Nan, J. Zhang, Z. Wei, ChemPhysChem 3 (2002) 898–901.
[27] H. Xu, L.P. Zeng, S.J. Xing, G.Y. Shi, J. Chen, Y.Z. Xian, L. Jin, Electrochem. Commun. 10 (2008) 1893–1896.
[28] K. Itaya, T. Ataka, S. Toshima, T. Shinohara, J. Phys. Chem. 86 (1982) 2415–2418.
[29] M.D. Stoller, S. Park, Y. Zhu, J. An, R.S. Ruoff, Nano Lett. 8 (2008) 3498–3502.
[30] M. Zhou, Y. Zhai, S. Dong, Anal. Chem. 81 (2009) 5603–5613.
[31] J. Wang, S. Yang, D. Guo, P. Yu, D. Li, J. Ye, L. Mao, Electrochem. Commun. 11 (2009) 1892–1895.
[32] D.A.C. Brownson, C.E. Banks, Analyst 135 (2010) 2768–2778.
[33] G. Zhang, F. Yang, M. Gao, X. Fang, L. Liu, Electrochim. Acta 53 (2008) 5155–5161.
[34] L. Fu, S.J. You, F. Yang, M. Gao, X. Fang, G. Zhang, J. Chem. Technol. Biotechnol. 85 (2010) 715–719.
[35] F. Li, H. Yang, C. Shan, Q. Zhang, D. Han, A. Ivaska, L. Niu, J. Mater. Chem. 19 (2009) 4022–4025.
[36] L. Liu, J.W. Lee, B.N. Popov, J. Power Sources 162 (2006) 1099–1103.
[37] Y. Wang, D. Zhang, H. Liu, J. Power Sources 195 (2010) 3135–3139.
[38] M.S. Ahmed, S. Jeon, J. Power Sources 218 (2012) 168–173.
[39] F. Wang, S. Hu, Electrochim. Acta 51 (2006) 4228–4235.
[40] A.A. Karyakin, E.E. Karyakina, L. Gorton, Electrochem. Commun. 1 (1999) 78–82.
[41] A.A. Karyakin, O.V. Gitelmacher, E.E. Karyakina, Anal. Chem. 67 (1995) 2419–2423.
[42] Y. Zou, L.X. Sun, F. Xu, Biosens. Bioelectron. 22 (2007) 2669–2674.